Axial Channeling in Electron Diffraction

A. Ichimiya * and G. Lehmpfuhl **

Fritz-Haber-Institut der Max-Planck-Gesellschaft, W.-Berlin

* Department of Applied Physics, Faculty of Engineering, Nagoya University, Nagoya, Japan

Z. Naturforsch. **33 a**, 269–281 (1978) ; received January 27, 1978

Kossel patterns from Silicon and Niobium were obtained with a convergent electron beam. An intensity maximum in the direction of the zone axes [001] and [111] of Nb was interpreted as axial channeling. The intensity distribution in Kossel patterns was calculated by means of the Bloch wave picture of the dynamical theory of electron diffraction. Particularly zone axis patterns were calculated for different substance-energy combinations and they were compared with experimental observations. The intensity distribution in the calculated Kossel patterns was very sensitive to the model of absorption and it was found that a treatment of the absorption close to the model of Humphreys and Hirsch [Phil. Mag. **18**, 115 (1968)] gave the best agreement with the experimental observations. Furthermore it is shown which Bloch waves are important for the intensity distribution in the Kossel patterns, how they are absorbed and how they change with energy.

Introduction

The intensity distribution in electron diffraction patterns from thick crystals depends in a characteristic way on the energy of the electrons and on the types of the scattering atoms. This phenomenon is closely related to electron channeling and was investigated in detail by Fujimoto et al. [1] for different kinds of crystals and different energies of the electrons up to 1 MeV. In electron micrographs of bend contours from wedge shaped crystals an energy dependence of the contrast was also observed [2] due to this phenomenon.

The energy dependence of the intensity distribution in electron diffraction patterns can be studied most clearly by taking Kossel patterns [3] produced by a widely opened cone of primary electrons. Experimentally this can be realized by placing the specimen in the back focal plane of a strong magnetic lens. A convergent beam with a cone angle of typically about 15° is then transmitted through the specimen. For high electron energies it becomes difficult to obtain such a widely opened electron beam. Fujimoto et al. [1] used in their experiments, mentioned above, a technique of Nakai [4], by which a widely opened electron beam can be produced at high energies by inelastic scattering of the electrons in a thin glas film which is placed in a short distance in front of the specimen.

Kossel patterns are in their appearance similar to Kikuchi patterns obtained from crystals which are so thick that the Laue spots including the spot due to the primary beam are already absent. In such Kikuchi experiments a widely opened electron beam is produced by multiple inelastic scattering in the crystal. For thinner crystals the interpretation of the intensity distribution may be more difficult because of the disturbance by Laue spots. The Kossel patterns, however, can be obtained already from relatively thin crystals, showing an intensity distribution undisturbed by Laue spots.

Gjønnes and Taftø [5] have shown that the characteristic intensity distribution in Kikuchi patterns produced by a primary electron beam parallel to some low indexed zone axis can be described by the Bloch wave picture of the dynamical theory including absorption. Such zone axis Kikuchi patterns were called 'channeling patterns'.

The scattering behaviour can be estimated due to Fujimoto et al. [6] by an interaction parameter

$$\alpha = \frac{\text{const}}{\sqrt{1-\beta^2}} \cdot \frac{Z}{N d^2}$$

which depends on the energy of the electrons (expressed by $\beta = v/c$), the atomic number Z, the distance d of the scattering atoms in the direction of the electron beam and the density N of atoms. In the dynamical theory of electron diffraction the relativistic potential of the crystal corresponds to that parameter.

Berry [7] and Kambe [8] applied the tight-binding methods of band theory to the scattering of electrons in a crystal near a low indexed zone axis. By this method the Bloch waves with marked concentration of the electrons at or near the rows of atoms are understood as bound states in the two dimensions perpendicular to the zone axis, cor-

** Abt. Prof. K. Molière.

Reprint requests to Dr. G. Lehmpfuhl, Fritz-Haber-Institut, Faradayweg 4–6, D-1000 Berlin 33.

responding to the classical picture of channeling. By calculating the energy-eigenvalues one can see which Bloch wave can be considered to be a bound state, a losely bound state, or a free Bloch wave. Due to the relativistic potential the shape of the Bloch waves, their excitation strength and their eigenvalues change with the electron energy and consequently change their inelastic interaction with the crystal. The characteristic energy dependence of the intensity distribution in Kikuchi-, Kossel- and Laue-patterns [1] can be well understood by this model.

During the analysis of the energy dependence of the two dimensional bound states of the electrons, travelling through some crystal, it was found that one should observe in the Kossel pattern of Ge an intensity maximum in the [001] direction with 1 MeV electrons. At this energy a Bloch wave is strongly excited having maximum density between the atom rows. This Bloch wave is weakly absorbed and should give rise to an enhanced transmission. This maximum in direction of the zone axis corresponds to the pronounced maximum in the direction of a lattice plane, observed by Humphreys et al. [2] and by Fujimoto et al. [9] by high-voltage electron microscopy. The bend contours of a gold crystal show intensity maxima for such crystal orientations, where the electron beam is parallel to the (111)-plane. This behaviour was called 'Bloch wave channeling'.

The expected intensity maximum in the direction of the [001]-zone axis of Ge was observed by Fujimoto et al. [1] with 1 MeV electrons, but usually at lower energies in Kossel patterns one observes an intensity minimum in the direction of the zone axis as was shown in different experiments [10]. At higher electron energies the intensity minimum in the Kossel pattern changes to an intensity maximum. The maximum is also visible in Kikuchi patterns even with a superimposed Laue spot pattern if the incident beam is slightly tilted against the zone axis (0.25 Θ-Bragg). The intensity maximum can be seen as a diffuse spot in the direction of the zone axis beside the peak which is due to the primary beam [1].

By means of the interaction parameter [6] one can estimate which crystals would have a similar scattering behaviour at what energies. It was found that Niobium should give a similar diffraction pattern with 100 keV electrons in [001] direction as Ge with 1 MeV electrons. Therefore, in the present work experiments were done with Nb in a normal diffraction camera with 100 keV electrons, in order to study the effects which are observed in Ge with 1 MeV electrons and to learn about the density distribution of different Bloch waves and to see how they are absorbed.

Theory

The intensity distribution in the Kossel patterns was calculated by the dynamical theory of electron diffraction due to Bethe [11] using the formalism described earlier [12]. The absorption of the electrons was taken into account by a complex scattering potential. The absorption coefficients of the Bloch waves were calculated from the imaginary part of the crystal potential by a perturbation method [13].

Reciprocity

To calculate the intensity distribution in the Kossel pattern we make use of the reciprocity theorem [14]. In Fig. 1 a an incident beam of intensity $I_0 = i_0\,\mathrm{d}\omega$ falling within a solid angle $\mathrm{d}\omega$ onto the crystal is scattered by the crystal in a cone of 2α aperture. The scattered intensity $I_s = i_s\,\mathrm{d}\omega$ which falls in a solid angle $\mathrm{d}\omega$ depends on the scattering direction. The integral over all scattered beams gives the total primary intensity

$$I_0 = \int_{2\alpha} i_s(\boldsymbol{K}_0, \boldsymbol{K}_s)\,\mathrm{d}\omega \qquad (1)$$

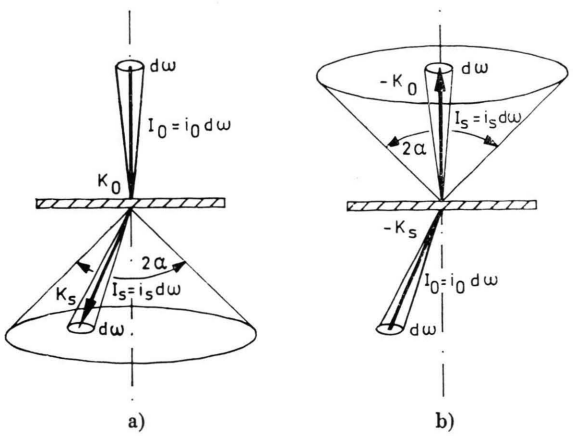

Fig. 1 a and b. Schematic diagram to illustrate the principle of reciprocity (see text). a) normal case of incidence, b) reciprocal case. Hatched area is the crystal.

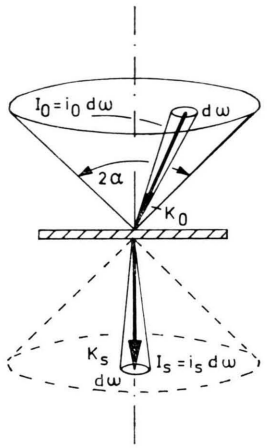

Fig. 2. Schematic diagram of a convergent-beam experiment to obtain a Kossel pattern.

where the first argument $\boldsymbol{K}_0$ of i_s indicates the wave vector of the primary beam and the second argument $\boldsymbol{K}_s$ the wave vector of the scattered beam. A reciprocal case is shown in Fig. 1 b for which due to the theorem of reciprocity

$$i_s(-\boldsymbol{K}_s, -\boldsymbol{K}_0) = i_s(\boldsymbol{K}_0, \boldsymbol{K}_s). \tag{2}$$

For the situation shown in Fig. 1 b Eq. (1) also holds.

Now we consider the situation in a convergent beam experiment in Figure 2. In the direction $\boldsymbol{K}_s$ we observe an intensity which is equal to the integral (1). If all scattered beams would remain within the cone of 2α aperture one would observe no contrast in the Kossel pattern because the integral (1) is independent of the direction of observation. The total intensity, however, is reduced by absorption and by elastic scattering of beams near the cone surface which are scattered into larger angles than 2α. One can take account for the last effect by introducing additional absorption. So the intensity we observe in a direction $\boldsymbol{S}$ in the Kossel pattern is given by Eq. (10) as is shown in the next paragraph. In the case of absorption we assume that the principle of reciprocity is also valid.

Intensity

The intensity of the primary electron beam I_0 is scattered in all the diffracted beams g having the intensity $I_g(z)$ which depends on the thickness z:

$$I_0 = \sum_g I_g(z). \tag{3}$$

The intensity of one diffracted beam g of a crystal of thickness z can be expressed by the amplitude of the diffracted beam

$$I_g(z) = \Psi_g^*(z) \cdot \Psi_g(z) \tag{4}$$

which depends on the partial waves $\Psi_g^{(i)}$ of the Bloch waves i

$$\Psi_g(z) = \sum_i \Psi_g^{(i)} \exp\left(\frac{2\pi i}{\lambda} \boldsymbol{S}_g^{(i)} \cdot \boldsymbol{N} \cdot z\right). \tag{5}$$

$\boldsymbol{N}$ is a unit vector perpendicular to the entrance surface of the crystal and $\boldsymbol{S}_g^{(i)}$ are normalized crystal wave vectors

$$\boldsymbol{S}_g^{(i)} = \boldsymbol{S}_e + \boldsymbol{B}_g + \boldsymbol{N} \cdot \tau_i$$

having different normal components τ_i for different Bloch waves. $\boldsymbol{B}_g$ is a vector in the reciprocal lattice and $\boldsymbol{S}_e$ a unit vector in the direction of the incident beam. The differences of the normal components were called 'Anpassungen' by Bethe and they are determined together with the partial wave amplitudes from the fundamental equations of the dynamical theory as eigenvalues. The partial wave amplitudes are related to the eigenvector components $C_g^{(i)}$ by the boundary conditions

$$\Psi_g^{(i)} = C_g^{(i)} \cdot C_0^{(i)*}. \tag{6}$$

The eigenvector components $C_0^{(i)}$ we call "excitation strength" with

$$\sum_i \Psi_0^{(i)} = \sum_i C_0^{(i)} \cdot C_0^{(i)*} = 1.$$

They obey the relations of orthonormality

$$\sum_i C_h^{(i)} \cdot C_g^{(i)*} = \delta_{gh}, \quad \sum_g C_g^{(i)} \cdot C_g^{(j)*} = \delta_{ij}. \tag{7}$$

With these relations the intensity can be written

$$I_g(z) = \sum_{i,j} C_0^{(i)*} C_g^{(i)} C_0^{(j)} C_g^{(j)*} \cdot \exp\left\{\frac{2\pi i}{\lambda} (\tau_i - \tau_j) z\right\}. \tag{8}$$

Because of the absorption each Bloch wave is damped with its own characteristic absorption coefficient μ_i and consequently each partial wave has to be multiplied with an exponential factor $\exp\{-\mu_i \cdot z/2\}$. The total scattered intensity I_t is then given by

$$I_t(z) = \sum_g I_g(z) = \sum_i C_0^{(i)*} \exp\{-\tfrac{1}{2}\mu_i z\} \cdot \sum_j C_0^{(j)} \exp\{-\tfrac{1}{2}\mu_j z\} \sum_g C_g^{(i)} C_g^{(j)*} \cdot \exp\left\{\frac{2\pi i}{\lambda} (\tau_i - \tau_j) z\right\}. \tag{9}$$

Without absorption this intensity is equal to the primary intensity. Because of the normalized eigenvectors which obey (7), in Eq. (9) only the components with $i=j$ contribute to the intensity. The intensity is now with $\Psi_0^{(i)} = |C_0^{(i)}|^2$

$$I_t(z) = \sum_i \Psi_0^{(i)} \exp(-\mu_i z). \tag{10}$$

Because of absorption this intensity depends on the thickness.

Absorption

The absorption was taken into account by an imaginary part of the structure potential having the same periodicity as the real potential. We tested different models for the relation between real and imaginary part by putting

$$V_g^{\text{im}} = V_g^{\text{real}}(A + B g - C g^2) + E. \tag{11}$$

This general form contains the absorption model due to Hirsch and Humphreys [15] as well as the proportional and the δ-function models of absorption. A, B, C and E are constants which were fitted by comparing calculated with experimental intensity distributions. The δ-function model may be replaced in a more general consideration by a Gaussian model as is discussed later.

The absorption coefficients μ_i were calculated by a perturbation method [13] putting

$$\mu_i = \frac{2me}{h^2} \int |b_i(r)|^2 \cdot V_{\text{im}}(r)\, dr. \tag{12}$$

Here m, e and h are usual physical constants and $b_i(r)$ is the Bloch function of the fast electrons:

$$b_i(r) = \sum_g C_g^{(i)} \exp\left(\frac{2\pi i}{\lambda} \mathbf{S}_g^{(i)} \mathbf{r}\right). \tag{13}$$

By use of the relation (13) we obtain

$$\mu_i = \frac{2\pi m e \lambda}{h^2} \sum_g \sum_h C_g^{(i)*} V_{g-h}^{\text{im}} C_h^{(i)}. \tag{14}$$

It was not neccessary to apply a more general and more accurate many beam calculation with the complex structure potential.

Calculation

The calculation of the intensity distribution in a Kossel pattern is done by use of the reciprocity theorem: We interchange the direction of observation with the direction of the incident electron beam. For this orientation eigenvectors and eigenvalues are calculated in a many beam calculation as described earlier [12] (see appendix).

Bloch Waves

For a better physical understanding of the intensity distribution in the Kossel pattern the electron density distribution

$$D_i(\mathbf{r}) = b_i(\mathbf{r}) \cdot b_i^*(\mathbf{r}) \tag{15}$$

in strong Bloch waves was calculated [17] and related to their absorption coefficients. In a more accurate discussion the current density should be considered. However, as it was shown earlier [16] it is sufficient to calculate the mean electron density of each Bloch wave describing the steady state of the electrons travelling through the crystal.

Experiments

The electron diffraction patterns were taken with a diffraction camera especially constructed in order to apply the Kossel-Möllenstedt technique. It is similar to a camera described by Mills et al. [18]. Kossel-Möllenstedt patterns can be taken from very small specimen areas of the order of 100 Å in diameter. In the case of Kossel patterns, however, the focus of the beam was several microns in diameter because of the spherical aberration of the lens and the large angle of the convergent beam cone.

With our camera Si and Nb were investigated. The Nb specimen were prepared by electrolytical polishing. The Nb-sheet was not annealed and the purity was 99.9%. The conditions for electropolishing were as follows: 175 ccm HF (40%), 175 ccm HNO_3 (63%) and 650 ccm H_2O; current density was 0.2 A cm^{-2} at a polishing potential of 7 V with Pt-cathode.

Results

Kossel patterns from Si and Nb taken with 100 keV electrons are shown in Figs. 3 a and b. The axis of the cone of the incident convergent electron beam was parallel to the [001] zone axis. The outer part of the Nb-Kossel pattern is disturbed by a lack of crystal perfection over the illuminated specimen area. The diameter of the crystal area contributing to the diffraction pattern was about 10 μ.

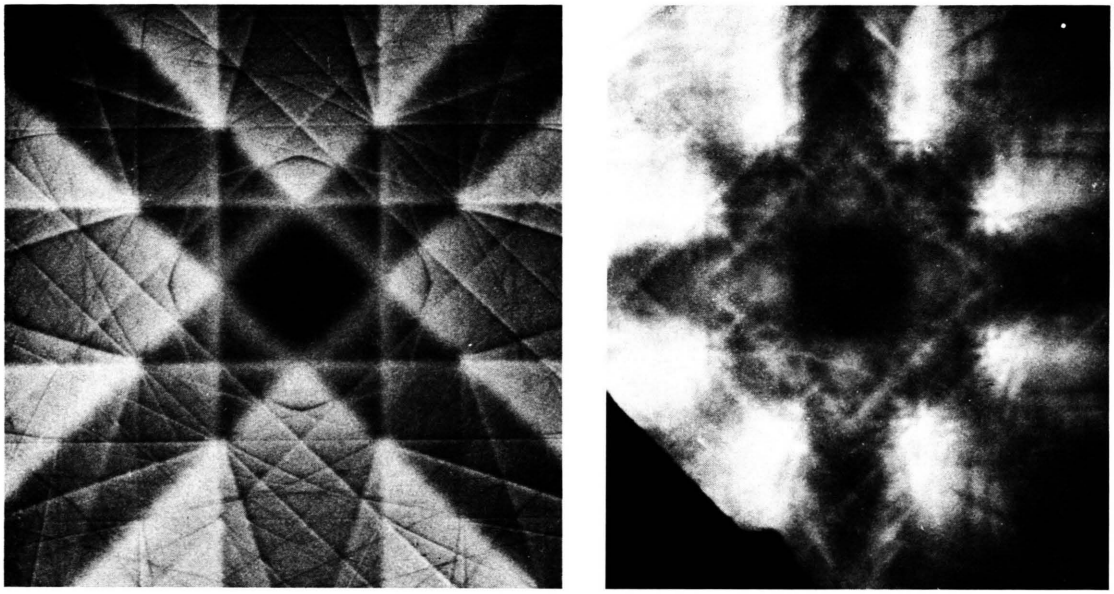

a b

Fig. 3 a and b. Kossel pattern from Si (a) and Nb (b) in [001] orientation obtained with 100 keV electrons.

The Si specimen was undistorted over this large area as may be seen in the Kossel pattern in Figure 3 a.

There is a characteristic difference between the two intensity distributions around the centres of the patterns. The square shaped dark part in the centre of the Nb-Kossel pattern has a faint intensity maximum. This maximum, the intensity distribution around the centre and the 8 strong intensity maxima are characteristic for energy-substance pairs represented by Nb at 100 keV. Very similar to this Kossel pattern from Nb is the Kossel pattern from Ge at 1 MeV [1]. The Kossel pattern in Fig. 3 b corresponds to a high voltage Kossel pattern of a light substance as Ge. The Kossel pattern from Ge at 100 keV looks similar to the Kossel patern from Si in Figure 3 a. In the square shaped dark part in the centre – standing on a corner – there is no intensity maximum. We see, however, dark streaks along the diagonals of the square. At high energies the shape of the dark streaks changes as in Figure 3 b.

In Figs. 4 and 5 the calculated intensity distributions are shown for Si and Nb for different absorption models and different thicknesses. The two-dimensional intensity distribution was displayed by the overprinting technique in a line printer output of a computer. 32 grey steps have been provided, however, in practice only between 20 steps can be distinguished. The resolution of the display is limited by the number of lines on a page and by the number of letters in a line.

In the calculation the following models for the absorption potential were used:

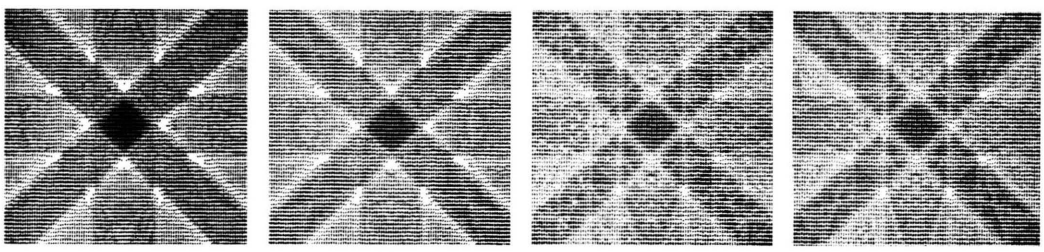

a b c d

Fig. 4. Calculated Kossel patterns (55-beam calculation) from Si in [001]-orientation for different models of absorption. Crystal thickness: 2000 Å, energy of the electrons: 100 keV. a: Model (1), b: Model (2), c: Model (3) with $D=0$, and d: Model (3) with $D=0.43$. For the calculations the values of Table I were used.

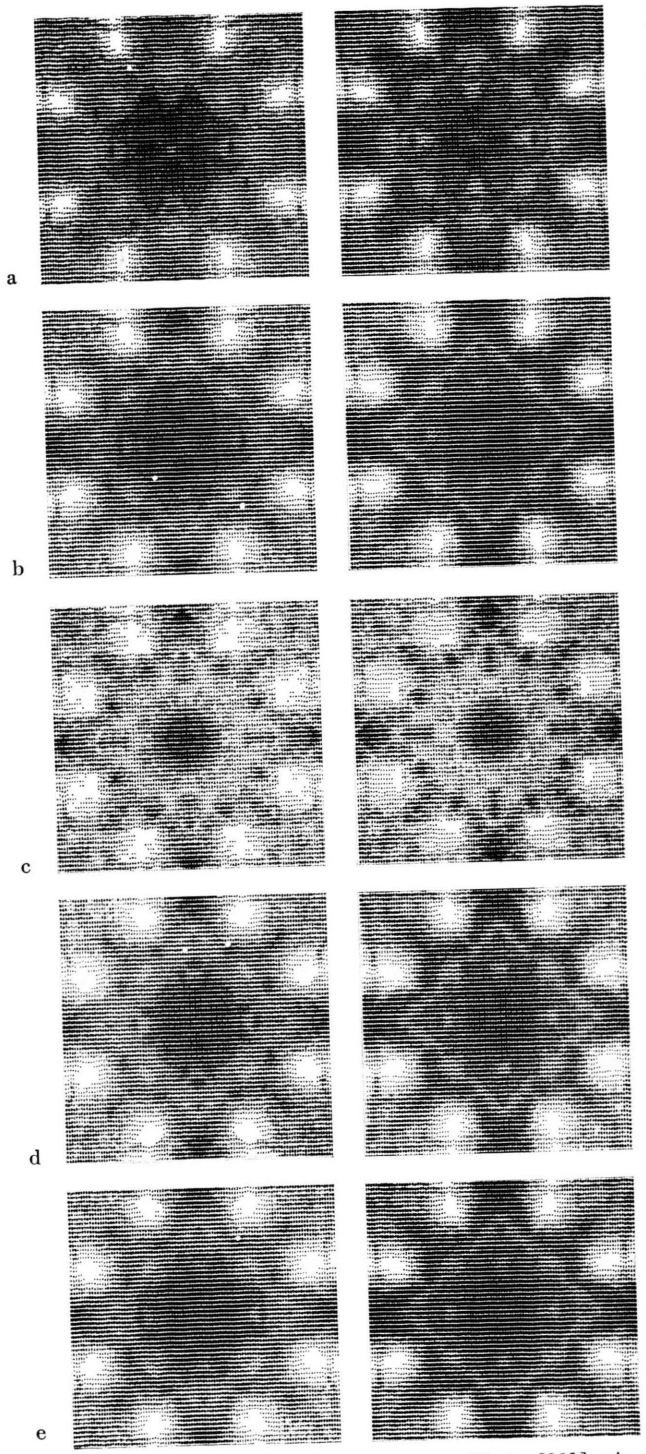

Fig. 5. Calculated Kossel patterns from Nb in [001]-orientation for two different thicknesses and different models of absorption. 55-beam calculation, energy of the electrons: 100 keV. Left column 1000 Å and right column 2000 Å. a: Model (1), b: Model (2), c–e: Model (3) with $D=0$ in c, D=0.7 in d, and $D=1$ in e. The calculations were done with the values of Table I.

1. Proportional model with $V_g^{\text{im}} = A \cdot V_g^{\text{real}}$.
2. Model close to the one due to Humphreys and Hirsch [15] which may be approximated by
$$V_g^{\text{im}} = (B\,g - C\,g^2) V_g^{\text{real}}.$$
3. Gaussian model which implies in its general form the δ-function model
$$V_g^{\text{im}} = \mathrm{F} \cdot \exp\left(-\frac{D\,g^2}{4\,d^2}\right) \sum_i \exp(2\pi i\, \boldsymbol{g} \cdot \boldsymbol{r}_i)$$

where d is the lattice constant and $\boldsymbol{r}_i$ the position of the i-th atom in the unit cell.

The calculated intensity distribution in the Si-Kossel pattern is not very sensitive to the absorption model and to the thickness. In Fig. 4 calculated Kossel patterns are shown for the different models of absorption from a thick Si crystal. The contrast of the Kossel lines increases with thickness. The geometric structure of the Kossel pattern seems to be best described by the Gaussian model with $D=0.43$. But also the model 2, due to Humphreys and Hirsch [15] shows the geometric structure. The Gaussian model with $D=0$ which corresponds to the δ-function model is physical nonrealistic and the calculated Kossel pattern shows an exaggerated geometric structure.

The calculated Nb-Kossel pattern in Fig. 5 is very sensitive to the thickness and also to the model of absorption. One criterion for the choice of the absorption model is the intensity maximum in the centre of the pattern in Fig. 3 b and another is the intensity distribution along the edges of the square surrounding this maximum which stands on a corner. The models (1) and (2) and the model (3) with large D-values give an intensity maximum in the centre. The appearance of this maximum depends strongly on the D-value of the Gaussian model as shown in Figure 6. For small D-values ($D=0$ or $D=0.43$) the intensity maximum in the direction of the [001]-zone axis is not reproduced, but with an increased value of D the intensity maximum appears. The calculated contrast of the intensity square surrounding this maximum is very weak using model (1). By the models (2) and (3) the intensity square is much better reproduced. Using model (3) the contrast of the intensity square decreases with increasing the value of D, and for a very large D-value the contrast may become very weak. Therefore the adequate absorption models are the model (2) and the model (3) with the optimum D-value; $D=1$. The eight intensity maxima

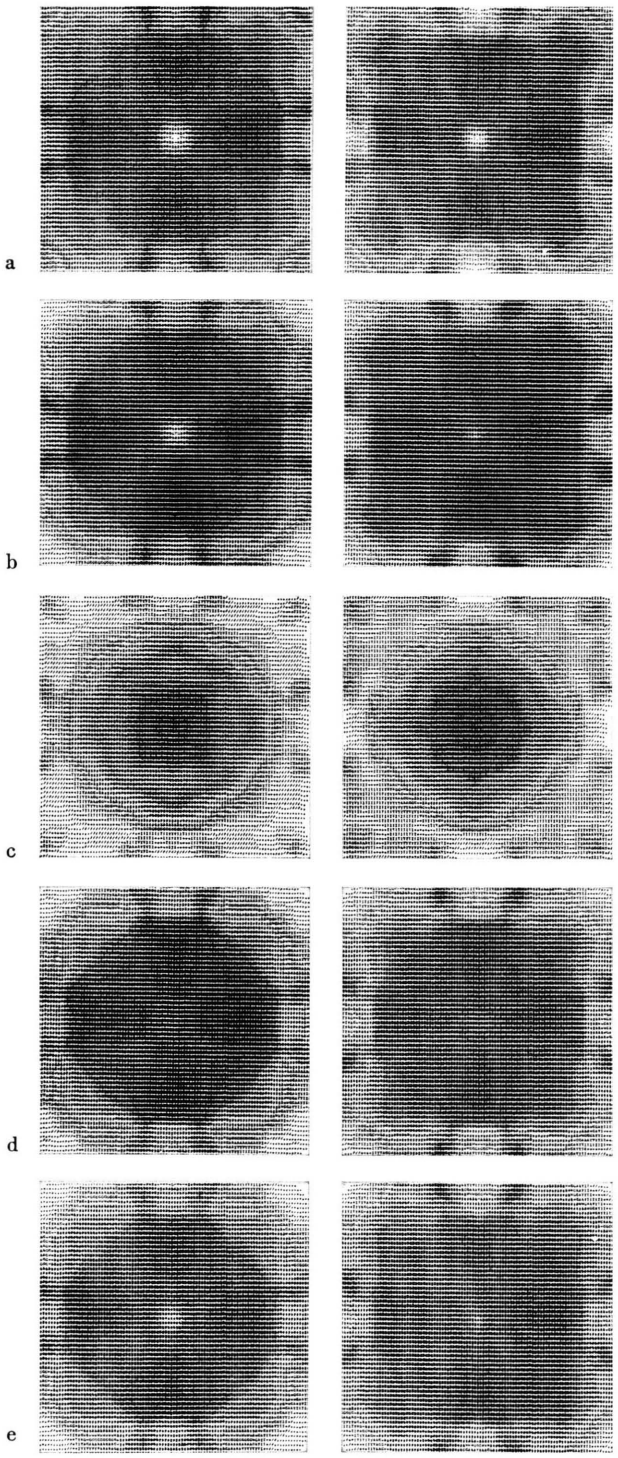

Fig. 6. Centre part of the calculated Nb-Kossel patterns in Fig. 5 showing the intensity distribution near the [001]-zone axis with better resolution, especially the appearance of the intensity maximum in the zone-axis direction.

in the outer part of the pattern are not sensitive to the absorption model.

The intensity distribution using model (3) with $D = 1.0$ is almost the same as the distribution using model (2) as can be seen in Figs. 5 and 6. This becomes understandable if we look at the imaginary potentials due to the different models. Fig. 7 shows the g-dependence of V_{im} of Nb for all of the models together with the theoretical values for Nb due to phonon excitation calculated by Radi [19]. Model (2) and model (3) with $D = 1.0$ give a similar g-dependence of the potential. For $D = 1.25$ the curves of the two models coincide. In Table I the parameters of the absorption models (2) and (3) giving the best fit are shown. In the last column parameters B and C of the approximation due to model (2) are shown, by which the imaginary potentials for Nb and Si published in the paper of Humphreys and Hirsch [15] are fitted. They differ a little from the experimentally determined parameters, indicating that only the tendency of the g-dependence of the absorption potential due to Humphreys and Hirsch is in agreement with the experimental observation.

The calculated distribution of the intensity near the centre can be shown very clear by displaying the intensity distribution with negative contrast as shown in Figure 8. The intensity maximum at the centre is here a black spot. The four intensity minima surrounding the intensity maximum in the centre in Fig. 3 b can be seen here very clear as white triangles.

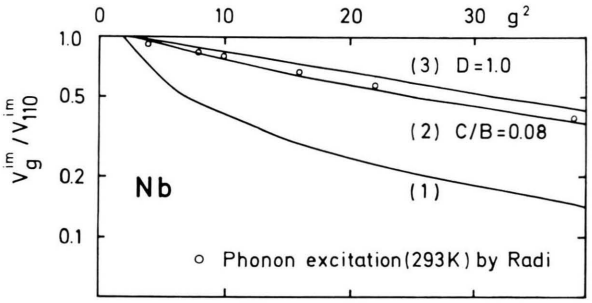

Fig. 7. Dependence of the Fourier-coefficients of the imaginary potential (absorption potential) on the absolute value of the vector g of the reciprocal lattice for different models of absorption (1), (2) and (3). The values due to phonon excitation by Radi are also indicated.

Discussion

The Gaussian model of the imaginary potential is very helpful to see how the imaginary potential

Table I.

Absorption model	(1)	(2)		(3)	Humphreys et al. [15]	
	A	*B*	*C*	*F*	*B*	*C*
Nb	0.07	0.055	0.0045	0.9	0.053	0.003
Si	0.009	0.0055	0.00045	0.27	0.009	0.0002

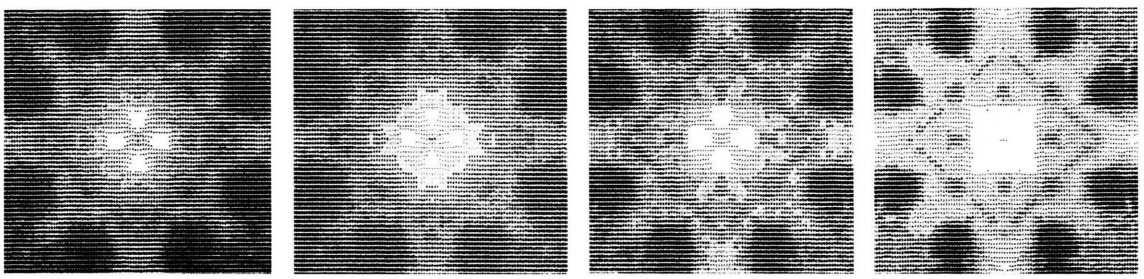

Fig. 8. Calculated Nb-Kossel patterns displayed with negative contrast to show the intensity distribution near the zone zone axis with better contrast. Calculatons were done with absorption model (2) for different thicknesses (500, 1000, 2000 and 4000 Å, from the left).

and the density distribution of Bloch waves act for the Kossel pattern, because the *D*-value of the Gaussian model gives directly the width of the imaginary potential at the atomic rows. The intensity maximum in the direction of the [001] zone axis can be interpreted by the superposition of the Gaussian potential and the Bloch-wave density distributions, because the absorption coefficient μ_i is given by the overlap-integral of the imaginary potential and the Bloch-wave density as shown in Equation (12).

It is interesting to display the density distribution of the electrons in the different Bloch waves for this particular situation and for other directions where characteristic maxima are observed. So the electron density in significant Bloch waves was calculated using the relation (15). Figure 9 shows the projection of the Nb-atoms onto the (001)-plane. The electron density was calculated for the hatched area containing three rows of Nb-atoms. Figure 10a shows 4 Bloch-waves with their characteristic density distributions. The direction of the incident electron beam is characterized by two parameters *G* and *H* explained in the appendix. The "excitation strength" of each Bloch wave is indicated in the line below the density distributions and the absorption coefficients of each Bloch-wave in the line above the density distributions. The absorption coefficients were calculated using model (2) for the absorption potential with the constants from Table I. The mean absorption was in this case assumed to be zero to show the effect of anomalous absorption already by the sign of the absorption coefficients. One can see imediately which Bloch waves suffer small absorption indicated by large "negative" absorption coefficients. Introducing the mean absorption all absorption coefficients become positive.

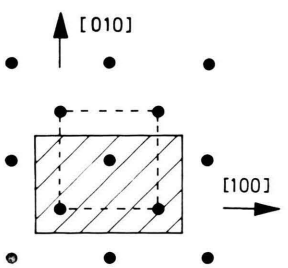

Fig. 9. Projection of the Nb-atoms onto the (001)-plane. The projection of the cubic unit cell is indicated by dashed lines. The electron density distribution of different Bloch waves was calculated for the hatched area.

For an incident electron beam parallel to the zone axis [001] which is characterized by $G = 0$ and $H = 0$ only the first and the fourth Bloch waves are excited. Bloch wave (1) with high density at the atom rows is most strongly absorbed for all of the models. For Bloch wave (4) the density is very small at the atom rows but otherwise uniformly distributed all over the projected area. The absorption coefficient of this Bloch wave is "negative".

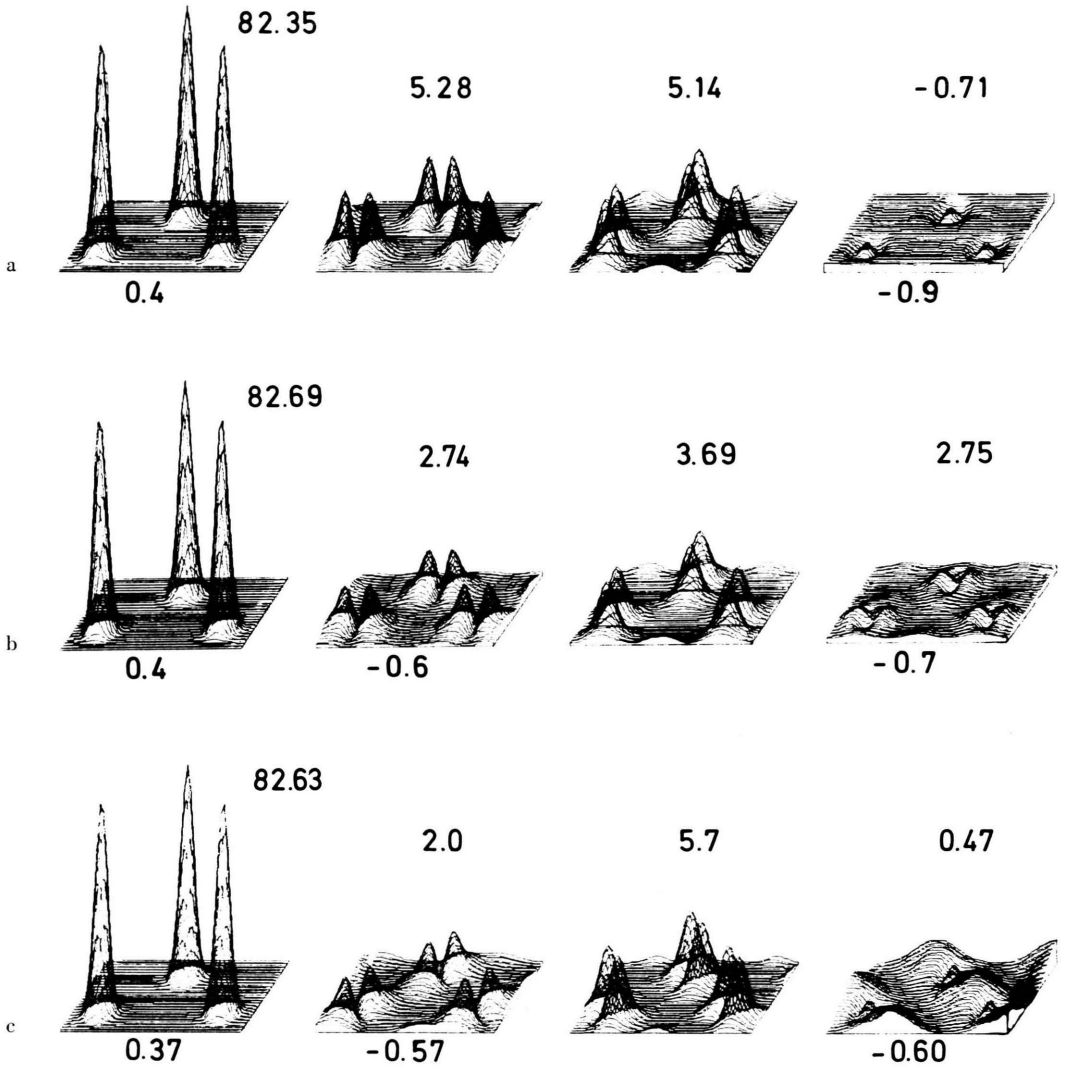

Fig. 10 a, b and c. Electron density distribution of 100 keV electron Bloch-waves in Nb. Only four Bloch waves are shown for three different orientations of the crystal. The number above each Bloch wave indicates its absorption coefficient in 10^3 Å-units and the number below is the "excitation strength". In a, the direction of the incident electron beam was parallel to the [001]-zone axis, characterized by $G=0$, $H=0$. In b. the incident beam was slightly tilted to $G=0$, H=1 and in c. to $G=1$, $H=1$.

If we tilt the direction of the incident electron beam, so that $G=0$ and $H=1$, Bloch wave (2) is excited with positive absorption coefficient and the absorption coefficient of Bloch wave (4) is increased up to 2.75 as it is shown in Figure 10 b. This results in an intensity minimum which can be seen in Fig. 3 b and which corresponds to the white triangle in Figure 8. For a direction of incidence characterized by G = 1 and $H=1$ Bloch wave (4) is less absorbed as can be seen in Figure 10 c. This results in a faint intensity between the white triangles in Fig. 8 which can also be seen in the Nb-Kossel pattern in Figure 3 b.

The Bloch waves for the direction of one of the eight intensity maxima in Fig. 3 b are shown in Fig. 11 characterized by $G=2.2$ and $H=4.2$. Many Bloch waves are excited. The strongest Bloch wave has the smallest absorption coefficient and shows the largest anomalous absorption. There are still two more Bloch waves carrying some intensity

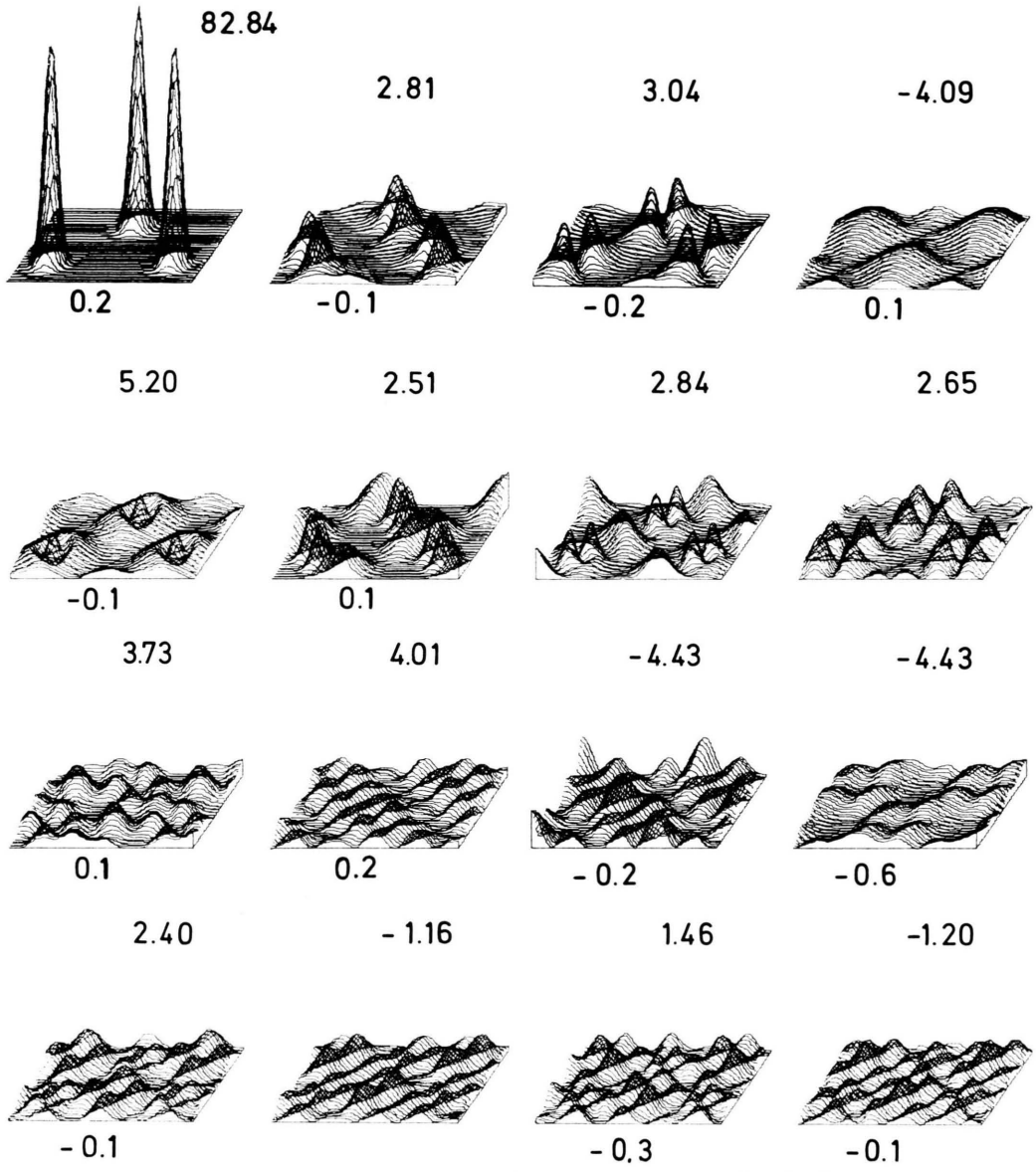

Fig. 11. Electron density distribution of 100 keV electron Bloch-waves in Nb. 16 Bloch waves are shown together with their absorption coefficients and their "excitation strength" (the numbers above and below resp. each Bloch wave). Orientation: $G=2.2$, $H=4.2$.

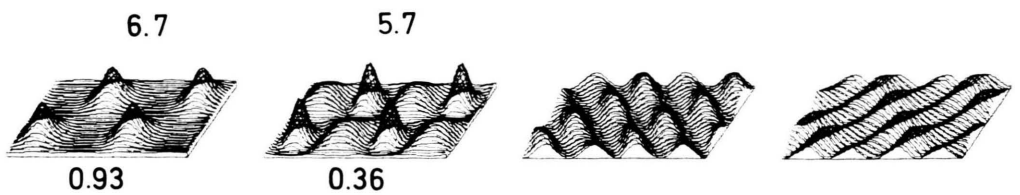

Fig. 12. Electron density distribution of 100 keV electron Bloch-waves in Si. At the orientation $G=0$, $H=0$ only two Bloch waves are excited having nearly the same absorption coefficients.

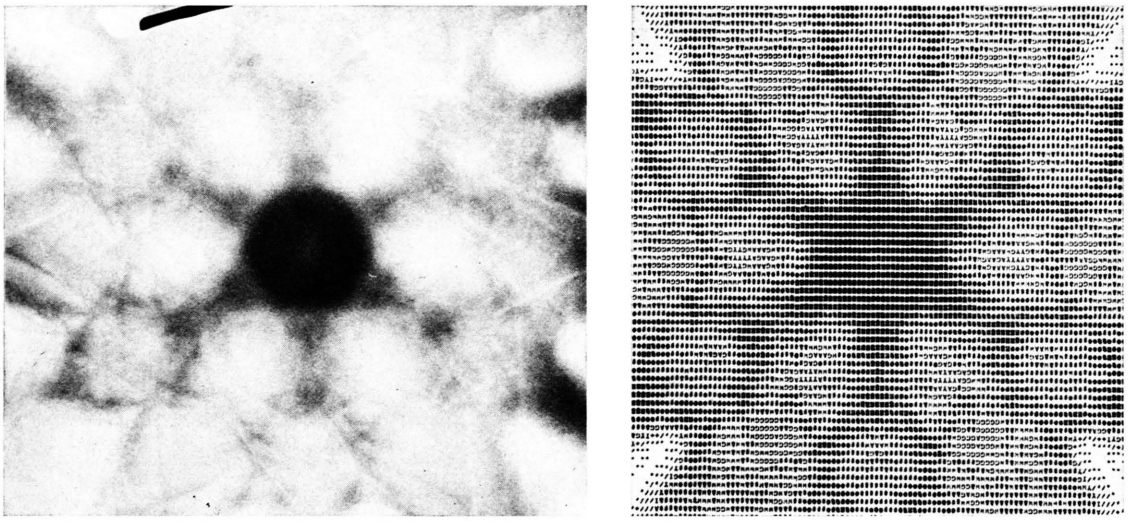

a b

Fig. 13. Kossel patterns from Nb in [111] orientation obtained with 100 keV electrons: a. Experiment, b. Calculation.

which suffer small absorption. 41% of the incident intensity is scattered into these Bloch waves. They are responsible for the characteristic intensity maxima. It is interesting to see that the three Bloch waves with small absorption coefficients have no density at the position of the atom rows.

The intensity minimum in the centre of the Si Kossel-pattern in Fig. 3 a we can also understand from such a Bloch-wave consideration. In Fig. 12 four Bloch waves are shown at 100 kV for $G = H = 0$. Bloch wave (1) is most strongly excited while Bloch wave (2), which corresponds to Bloch wave (4) in the case of Nb, is less excited with large absorption. So the electrons suffer large absorption in Si at 100 keV and we observe an intensity minimum in the direction of the [001] zone axis as it is shown in Figure 3 a. From the Bloch-wave picture we understand that the calculated intensity distribution in Si Kossel-patterns at 100 keV is not very sensitive to the model of absorption because the density peaks of the Bloch waves at the position of the atoms are not very sharp. The Bloch waves in Ge at 100 keV are very similar to these Bloch waves in Si. So we can understand that the Kossel pattern from Ge at 100 keV is similar to the Si Kossel-pattern in Figure 3 a. Since the Kossel pattern of Ge at 1 MeV becomes similar to the one of Nb at 100 keV, we expect to observe a similar Kossel pattern from Si at a high electron energy. Calculations have shown that this energy should be at 2.5 MeV.

Fujimoto et al. [1] have shown that the Nb-like Kossel patterns can be observed from other materials at characteristic energies as for Cu at 750 keV and for Fe at 350 keV. The Kikuchi pattern from Au – 50% Pd at 100 keV shown by Gjønnes [5] is also similar to the Nb-Kossel pattern. The interaction parameters due to Fujimoto et al. [6] are for four conditions:

$\alpha(\text{Nb}, 100\,\text{keV}) = 4.9$, $\alpha(\text{Ge}, 1\,\text{MeV}) = 4.1$,
$\alpha(\text{Cu}, 750\,\text{keV}) = 4.04$ and $\alpha(\text{Fe}, 350\,\text{keV}) = 3.8$.

We see that they fairly agree with each other, especially the last three values. During this analysis it was found that very similar electron density distributions in the Bloch waves exist in the four cases. Consequently the calculated Kossel patterns are very similar.

As a final test of the absorption model due to Humphreys and Hirsch the intensity distribution in theNb-Kossel pattern for the [111] zone axis was calculated and compared with an experimental observation in Figure 13. For this calculation the values of Table I were used. The agreement is fairly good even the faint maximum at the centre is reproduced.

Summary

The analysis of the energy dependence of the intensity distribution in Kossel patterns allows a

better understanding of the mechanism of electron absorption in crystals and it was found that these Kossel patterns can only be understood by considering the absorption. The intensity maximum which was observed in the direction of the zone axis for characteristic substance-energy combinations can be understood as axial channeling. It was confirmed that the Bloch-wave treatment of the scattering process is an adequate method of describing electron channeling phenomena.

We wish to thank Dr. K. Kambe and Prof. F. Fujimoto for many stimulating discussions, Dr. P. J. Smith for providing us with the Si specimen and Dr. P. L. Fejes for his help in programing the line printer display. One of us, A. I., wants to thank the MPG for financial support during his stay at the Fritz-Haber-Institut.

Appendix

The direction of observation in the Kossel pattern which corresponds due to reciprocity to the direction of the incident electron beam in the calculation was characterized by two parameters G and H, used already earlier [17]. These parameters are the intersection points of the Ewald sphere with two orthogonal axes in the reciprocal plane containing the diffraction pattern.

The calculation procedure was economized using the symmetry of the crystal. In a 55-beam calculation the eigenvalues and eigenvectors were calculated for 66 points in 1/8 of the first Brillouin zone (see Figure 14). The eigenvalues and eigenvectors of the full Brillouin zone were then determined by symmetry operations. We consider a plane in the reciprocal lattice which is perpendicular to the [001] zone axis containing the origin of the reciprocal lattice. This plane represents the diffraction pattern. In Fig. 14 one quarter of this reciprocal plane representing one quarter of the Kossel pattern is shown. The two parameters G and H are indicated. The Kossel patterns in Figs. 3 a and 3 b cover an area in the reciprocal (001) plane which

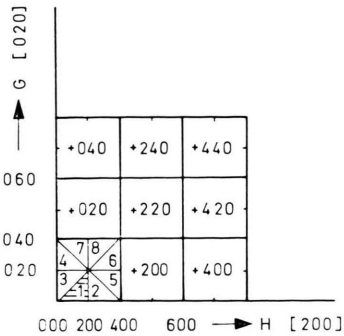

Fig. 14. One quarter of the reciprocal (001)-plane representing one quarter of the Kossel-pattern area. H and G are the intersection coordinates of the axes [200] and [020] in the reciprocal lattice with the Ewald sphere. The direction of the incident electron beam is determined by these coordinates. The primary calculation was done for 66 points in the hatched area (1) of the first Brillouin zone for a choosen set of reflections (h, k, l). The eigenvector amplitudes for the other areas are obtained by transforming the $h\,k\,l$ in the indicated way:
(1) Primary calculation with (h, k, l).
Transformations:
(2) $(h, k, l) \rightarrow (2-h, k, l)$,
(3) $(h, k, l) \rightarrow (k, h, l)$,
(4) $(h, k, l) \rightarrow (k, 2-h, l)$,
(5) $(h, k, l) \rightarrow (2-k, h, l)$,
(6) $(h, k, l) \rightarrow (2-k, 2-h, l)$,
(7) $(h, k, \mathrm{l}) \rightarrow (h, 2-k, l)$,
(8) $(h, k, l) \rightarrow (2-h, 2-k, l)$.

can be marked by $-12 \leqq G \leqq 12$ and $-12 \leqq H \leqq 12$.

The calculation was done for 66 points (G, H) in the hatched area ① of the first Brillouin zone for a defined set of reflections $(h\,k\,l)$, the zero beam included, giving the eigenvector components $C_g^{(i)}$. The step width for the different calculations was $\Delta H = \Delta G = 0.2$. The eigenvector components for the other areas were then determined from the eigenvectors of area ① by the indicated transformations of the reflection indices. The intensity is due to Eq. (10) given by the new eigenvector components with zero index $C_0^{(i)}$. From the eigenvectors of these 8 areas the full data field was then determined by further transformations (indicated) and applying the boundary conditions. However, the accuracy of the results of this procedure is limited by the number of beams used in the primary many beam calculation.

[1] F. Fujimoto, Y. Uchida, and G. Lehmpfuhl, Quatrieme Congr. Intern., Toulouse 1975, p. 109–112.
[2] C. J. Humphreys, L. E. Thomas, J. S. Lally, and R. M. Fisher, Phil. Mag. **23,** 87 (1971).
[3] P. Goodman, Acta Cryst. **A 28,** 92 (1974).
[4] Y. Nakai, Acta Cryst. **A 26,** 459 (1970).
[5] J. Gønnes and J. Taftø, Nucl. Instrum. Methods **132,** 141 (1976).
[6] F. Fujimoto, S. Takagi, K. Komaki, H. Koike, and Y. Uchida, Radiaton Effects **12,** 153 (1972).

[7] M. V. Berry, J. Physics c **4,** 697 (1971).
[8] K. Kambe, G. Lehmpfuhl, and F. Fujimoto, Z. Naturforsch. **29 a,** 1034 (1974).
[9] F. Fujimoto, N. Sumoda, and H. Fujita, J. Phys. Soc. Japan **42,** 1274 (1977).
[10] F. Fujimoto and G. Lehmpfuhl, Z. Naturforsch. **29 a,** 1929 (1974).
[11] H. Bethe, Ann. Physik Leipzig **87,** 55 (1928).
[12] G. Lehmpfuhl and A. Reissland, Z. Naturforsch. **23 a,** 544 (1968).
[13] A. Ichimiya, Japan. J. Appl. Phys. **8,** 518 (1969); P. B. Hirsch, A. Howie, R. B. Nicholson, D. W. Pashley, and M. J. Whelan, Electron Microscopy of Thin Crystals, Butterworths, London, p. 217.
[14] A. P. Pogany and P. S. Turner, Acta Cryst. **A 24,** 103 (1968).
[15] C. J. Humphreys and P. B. Hirsch, Phil. Mag. **18,** 115 (1968).
[16] K. Ishida, A. W. S. Johnson, and G. Lehmpfuhl, Z. Naturforsch. **30 a,** 1715 (1975).
[17] G. Lehmpfuhl, Z. Naturforsch. **28 a,** 1 (1973).
[18] D. J. H. Cockayne, P. Goodman, J. C. Mills, and A. F. Moodie, Rev. Sci. Instrum. **38,** 1097 (1967).
[19] G. Radi, Acta Cryst. **A 26,** 41 (1970).